Vol 17 No 12, December 2008
1674-1056/2008/17(12)/4492-06

Chinese Physics B

© 2008 Chin. Phys. Soc.
and IOP Publishing Ltd

Quantum interference in laser-assisted photo-ionization excited by a femtosecond x-ray pulse*

Ge Yu-Cheng(葛愉成)†

School of Physics and State Key Laboratory of Nuclear Physics and Technology, Peking University, Beijing 100871, *China*

(Received 23 May 2008; revised manuscript received 1 July 2008)

The photoelectron energy spectra (PESs) excited by monochromatic femtosecond x-ray pulses in the presence of a femtosecond laser are investigated. A PES is composed of a set of separate peaks, showing interesting comb-like structures. These structures result from the quantum interferences between photoelectron wave packets generated at different times. The width and the localization of each peak as well as the number of peaks are determined by all the laser and x-ray parameters. Most of peak heights of the PES are higher than the classical predictions.

Keywords: femtosecond x-ray pulse, photo-ionization, quantum interference, photoelectron energy spectrum

PACC: 3365, 3280F, 3280, 3365C

1. Introduction

Since the successful experiment on the generation of 650-attosecond isolated extreme ultraviolet (xuv) pulses was reported,[1,2] direct and accurate measurement of attosecond xuv has become a popular topic in this respect.[3−10] However, measuring the temporal profile of a femtosecond (1fs= 10^{-15} s) soft x-ray remains a challenge which has greatly restricted the applications of such pulses in chemical and biological researches. This may partly be ascribed to the lack of the non-linear effect to be used to measure the femtosecond x-ray pulse and the difficulty in interpreting the measured photoelectron energy spectra (PESs). Because the duration of an attosecond x-ray pulse is less than one laser optical cycle, calculation shows that the PES is relatively simple.[11] In contrast, a femtosecond x-ray pulse spans many laser optical cycles, and the calculated PES is more complicated. It is interesting to theoretically investigate the PESs generated at different photon energies of femtosecond x-ray pulses, and to compare them with their classical predictions to show how the quantum effect plays a role in laser-assisted femtosecond x-ray photo-ionization.

In this paper, the PESs are calculated for femtosecond x-ray pulses in the presence of a strong short laser. Using a cross correlation between two light beams in hydrogen atoms, the x-ray is temporally adjusted to the laser envelope, and the photoelectrons are collected at an observation angle (θ) of zero degree, i.e. $\theta = 0°$ (θ is defined as the angle between the photoelectron momentum and the direction of laser polarization).

2. Strong field approximation

In a cross correlation between a femtosecond x-ray pulse and a dressing laser pulse, the electron motion satisfies the time-dependent Shrödinger equation in atomic units

$$\mathrm{i}\frac{\partial}{\partial t}\Psi(\boldsymbol{r},t) = \left[-\frac{1}{2}\nabla^2 - \frac{1}{r} - \boldsymbol{r}E(t)\right]\Psi(r,t), \qquad (1)$$

where $\boldsymbol{r} = (x, y, z)$ denotes the space coordinates, and $\Psi(\boldsymbol{r}, t)$ represents the electron wave function. The electric field $\boldsymbol{E}(t) = \boldsymbol{E}_{\mathrm{l}}(t) + \boldsymbol{E}_{\mathrm{x}}(t)$ comprises the contribution of a linearly polarized laser, $\boldsymbol{E}_{\mathrm{l}}(t) = E_{\mathrm{l}}(t)\cos(\varpi_{\mathrm{l}}t + \Phi)$ in the x direction with Φ being the carrier-envelope phase, and an x-ray, $\boldsymbol{E}_{\mathrm{x}}(t) = E_{\mathrm{x}}(t)\cos(\varpi_{\mathrm{x}}t)$ in the x direction, where ϖ_{l} and ϖ_{x} are the laser and x-ray angular frequencies, respectively. $E_{\mathrm{l}}(t) = E_0F(t)$, where $F(t)$ is the envelope function of the laser electric field, and E_0 is the amplitude. The electric field is related to the vector potential $\boldsymbol{A}(t)$ by $\boldsymbol{E}(t) = -(1/c)\partial_t\boldsymbol{A}(t)$, where c is the light velocity in vacuum.

*Project supported by the National Natural Science Foundation of China (Grant No 10675014).

†Corresponding author. E-mail: gyc@pku.edu.cn

Equation (1) can be solved analytically by applying the strong field approximation (SFA).[12,13] As a result, the Coulomb continuum eigenfunctions may be substituted by plane waves, and Eq.(1) is integrated by using the expression $\Psi(\boldsymbol{r},t) = \mathrm{e}^{\mathrm{i}I_p t}\left(|0\rangle + \int \mathrm{d}^3\boldsymbol{p} b(\boldsymbol{p},t)\,|\boldsymbol{p}\rangle\right)$. Here $|0\rangle$ denotes the atomic ground state with ionization potential I_p. The plane wave is given by $|\boldsymbol{p}\rangle = \exp(\mathrm{i}\boldsymbol{p}\cdot\boldsymbol{r})$, in which $\boldsymbol{p}$ is the electron momentum, and $b(\boldsymbol{p},t)$ is the momentum space wave function of free electrons. Within the SFA, the probability amplitude for the transition from $|0\rangle$ to a final state $|\boldsymbol{p}\rangle$ reads

$$b(\boldsymbol{p}) = \mathrm{i}\int_{-\infty}^{\infty} \mathrm{d}t E(t)\mathrm{d}_x[\boldsymbol{p}-\boldsymbol{A}(t)]\mathrm{e}^{-\mathrm{i}\widetilde{S}(t)}, \qquad (2)$$

where $\widetilde{S}(t)$ is the quasi-classical action

$$\widetilde{S}(t) = \int_t^{\infty} \mathrm{d}t' \left\{\frac{[\boldsymbol{p}-\boldsymbol{A}(t')]^2}{2} + I_p\right\}. \qquad (3)$$

$\boldsymbol{d}(\boldsymbol{p}) = \langle \boldsymbol{p}\,|x|\,0\rangle$ is the atomic dipole matrix element for the bound-free transition, and $d_x(\boldsymbol{p})$ is the component parallel to the polarization axis. $\boldsymbol{d}(\boldsymbol{p}) = \mathrm{i}2^{7/2}\alpha^{5/4}\boldsymbol{p}/\pi(2I_p+\boldsymbol{p}^2)^3$ for the hydrogen bound s state ($\alpha = 2I_p$, and $I_p = 13.6\,\mathrm{eV}$). Physically, Eq.(2) describes quantum interferences between electron wave packets generated at different times.

3. Photoelectron energy spectrum

The photoelectron momentum spectrum (PMS) is given by $|b(\boldsymbol{p})|^2$. Mathematically, $b(\boldsymbol{p})$ can be expanded into four terms,

$$b(\boldsymbol{p}) = b_1(\boldsymbol{p}) + b_2(\boldsymbol{p}) + b_3(\boldsymbol{p}) + b_4(\boldsymbol{p}), \qquad (4)$$

where

$$\begin{aligned}
b_1(\boldsymbol{p}) &= \frac{1}{2}\mathrm{i}\int_{-\infty}^{\infty} \mathrm{d}t E_{\mathrm{x}}(t)\mathrm{d}_x[\boldsymbol{p}-\boldsymbol{A}(t)]\mathrm{e}^{-\mathrm{i}\widetilde{S}_1(t)},\\
b_2(\boldsymbol{p}) &= \frac{1}{2}\mathrm{i}\int_{-\infty}^{\infty} \mathrm{d}t E_{\mathrm{x}}(t)\mathrm{d}_x[\boldsymbol{p}-\boldsymbol{A}(t)]\mathrm{e}^{-\mathrm{i}\widetilde{S}_2(t)},\\
b_3(\boldsymbol{p}) &= \frac{1}{2}\mathrm{i}\int_{-\infty}^{\infty} \mathrm{d}t E_{\mathrm{l}}(t)\mathrm{d}_x[\boldsymbol{p}-\boldsymbol{A}(t)]\mathrm{e}^{-\mathrm{i}\widetilde{S}_3(t)},\\
b_4(\boldsymbol{p}) &= \frac{1}{2}\mathrm{i}\int_{-\infty}^{\infty} \mathrm{d}t E_{\mathrm{l}}(t)\mathrm{d}_x[\boldsymbol{p}-\boldsymbol{A}(t)]\mathrm{e}^{-\mathrm{i}\widetilde{S}_4(t)}, \qquad (5)
\end{aligned}$$

and

$$\begin{aligned}
\widetilde{S}_1(t) &= \int_t^{\infty} \mathrm{d}t' \left\{[\boldsymbol{p}-\boldsymbol{A}(t')]^2/2 - (\varpi_{\mathrm{x}} - I_p)]\right\},\\
\widetilde{S}_2(t) &= \int_t^{\infty} \mathrm{d}t' \left\{[\boldsymbol{p}-\boldsymbol{A}(t')]^2/2 + (\varpi_{\mathrm{x}} + I_p)\right\},\\
\widetilde{S}_3(t) &= \int_t^{\infty} \mathrm{d}t' \left\{[\boldsymbol{p}-\boldsymbol{A}(t')]^2/2 - (\varpi_{\mathrm{l}} - I_p)\right\},\\
\widetilde{S}_4(t) &= \int_t^{\infty} \mathrm{d}t' \left\{[\boldsymbol{p}-\boldsymbol{A}(t')]^2/2 + (\varpi_{\mathrm{l}} + I_p)\right\}. \qquad (6)
\end{aligned}$$

$\widetilde{S_j}(t)(j = 1,2,3,4)$ are the quasi-classical actions of $b_j(\boldsymbol{p})$.

The terms $b_1(\boldsymbol{p}) + b_2(\boldsymbol{p})$ describe the amplitude of x-ray-induced photo-ionization. Because the factor $\mathrm{e}^{-\mathrm{i}\widetilde{S}_1(t)}$ varies much faster than others entering $b_1(\boldsymbol{p})$, the dominant contribution to the integral over t in $b_1(\boldsymbol{p})$ comes from the stationary points $t_{\mathrm{st},n}$ ($n = 1,2,3,\ldots$),

$$\begin{aligned}
&\frac{\mathrm{d}}{\mathrm{d}t}\widetilde{S}_1(t)\,\big|_{t=t_{\mathrm{st},n}}\\
&= -\left\{\frac{[\boldsymbol{p}-\boldsymbol{A}(t_{\mathrm{st},n})]^2}{2} - (\varpi_{\mathrm{x}} - I_p)\right\} = 0. \qquad (7)
\end{aligned}$$

In fact, Eq.(7) is the energy conservation law which determines initial kinetic energy of the generated electron. For an attosecond x-ray pulse which is temporally located close to $t = 0$ ($\Phi = 0°$) and whose duration is less than half a laser optical cycle, there is only one stationary point (i.e. $n = 1$) that satisfies Eq.(7). For a femtosecond x-ray pulse which spans many laser optical cycles, there are many stationary points ($n > 1$).

Since the factor $\mathrm{e}^{-\mathrm{i}\widetilde{S}_2(t)}$ varies much faster than others entering $b_2(\boldsymbol{p})$, the dominant contribution to the integral in $b_2(\boldsymbol{p})$ comes from the stationary points $t'_{\mathrm{st},n}$ ($n = 1,2,3,\ldots$),

$$\begin{aligned}
&\frac{\mathrm{d}}{\mathrm{d}t}\widetilde{S}_2(t)\,\big|_{t=t'_{\mathrm{st},n}}\\
&= -\left\{\frac{[\boldsymbol{p}-\boldsymbol{A}(t'_{\mathrm{st},n})]^2}{2} + (\varpi_{\mathrm{x}} + I_p)\right\} = 0. \qquad (8)
\end{aligned}$$

However, Eq.(8) has no real solutions of $t'_{\mathrm{st},n}$. At the stationary points $t_{\mathrm{st},n}$ ($n = 1,2,3,\ldots$), $b_2(\boldsymbol{p})$ can be neglected as compared with $b_1(\boldsymbol{p})$.

The terms $b_3(\boldsymbol{p}) + b_4(\boldsymbol{p})$ describe the amplitude of laser-induced photo-ionization. Similar to $b_2(\boldsymbol{p})$, both $b_3(\boldsymbol{p})$ and $b_4(\boldsymbol{p})$ have no real solutions of the stationary points. At the stationary points $t_{\mathrm{st},n}$ ($n = 1,2,3,\ldots$), $b_3(\boldsymbol{p})$ and $b_4(\boldsymbol{p})$ can be neglected as compared with $b_1(\boldsymbol{p})$. Therefore,

$$b(\boldsymbol{p}) \approx b_1(\boldsymbol{p}). \qquad (9)$$

Finally, at the stationary points $t_{\mathrm{st},n}$ ($n = 1,2,3,\ldots$), we have

$$b(\boldsymbol{p}) = \sum_n b_1(\boldsymbol{p}, t_{\mathrm{st},n}) + \varepsilon, \qquad (10)$$

where

$$\varepsilon = b(\boldsymbol{p}) - \sum_n b_1(\boldsymbol{p}, t_{\mathrm{st},n}). \tag{11}$$

The first term on the right-hand side of Eq.(10) is called the classical term, and ε is a residual term which depicts the oscillation structure of $b(\boldsymbol{p})$ because of the phase factor in Eq.(2), $\mathrm{e}^{-\mathrm{i}\widetilde{S}(t)}$.

At the stationary points $t_{\mathrm{st},n}$ $(n = 1, 2, 3, \ldots)$, $b_1(\boldsymbol{p})$ can be expressed as

$$\begin{aligned} & b_1(\boldsymbol{p}, t_{\mathrm{st},n}) \\ = & \sqrt{\frac{\pi}{2\mathrm{i}d^2\widetilde{S}_1(t)/dt^2\,|_{t=t_{\mathrm{st},n}}}} \\ & \times E_{\mathrm{x}}(t_{\mathrm{st},n}) d_x[\boldsymbol{p} - \boldsymbol{A}(t_{\mathrm{st},n})] \mathrm{e}^{-\mathrm{i}\widetilde{S}_1(t_{\mathrm{st},n})}. \end{aligned} \tag{12}$$

Thus $|b(\boldsymbol{p})|^2$ can be expanded into four terms $(n, m = 1, 2, 3, \ldots)$,

$$\begin{aligned} |b(\boldsymbol{p})|^2 = & \sum_{n,m} b_1(\boldsymbol{p}, t_{\mathrm{st},n}) b_1^*(\boldsymbol{p}, t_{\mathrm{st},m}) \\ & + \sum_n b_1(\boldsymbol{p}, t_{\mathrm{st},n}) \varepsilon^* \\ & + \sum_n b_1^*(\boldsymbol{p}, t_{\mathrm{st},n}) \varepsilon + \varepsilon\varepsilon^*. \end{aligned} \tag{13}$$

The first term on the right-hand side of Eq.(13) represents the classical prediction of the PMS, and the remaining three terms describe the oscillation structures of the PMS.

Because the quasi-classical action $\tilde{S}_1(t)$ is a pulse integral, it is difficult to have an analytical form of $|b(\boldsymbol{p})|^2$. The PES, $n(W)$, is defined as the number of photoelectrons collected at an energy W per unit energy. $n(W)$ can be easily converted from PMS (the number of collected photoelectrons per unit momentum), into $|b(\boldsymbol{p})|^2$, i.e. $n(W) = \sqrt{m_e/2W}\,|b(\boldsymbol{p})|^2$, where m_e is the electron mass and $W = \sqrt{\boldsymbol{p}^2/2m_e}$. The initial kinetic energy of the photoelectron is $W_0 = \hbar\varpi_{\mathrm{x}} - I_p$, where $\hbar$ is set to be 1 in the following for simplicity. We numerically calculate PESs and their classical predictions for comparison.

4. Calculation

In schematic calculations, a laser with a wavelength (λ_{l}) of 750 nm, i.e.$\lambda_{\mathrm{l}} = 750$ nm and $\Phi = 0°$ is used. $F(t) = \exp[-4\ln 2 \cdot (t)^2/\tau_{\mathrm{l}}^2]$ is a Gaussian function with a time duration (τ_{l}) of 400 fs, i.e. $\tau_{\mathrm{l}} = 400$ fs in full width at half maximum (FWHM). The peak laser intensity is $S = 1 \times 10^{14}\,\mathrm{W/cm^2}$. A $\tau_{\mathrm{x}} = 50$ fs (time duration in FWHM) and $\varpi_{\mathrm{x}} = 120$ eV (centre energy) Gaussian shape x-ray pulse is temporally centred at the time point t_N= 169.86 fs (falling-side laser envelope). Figure 1(a) illustrates the cross correlation between x-ray and laser, and shows laser-related functions and the x-ray intensity profile, $f(t)$. Figure

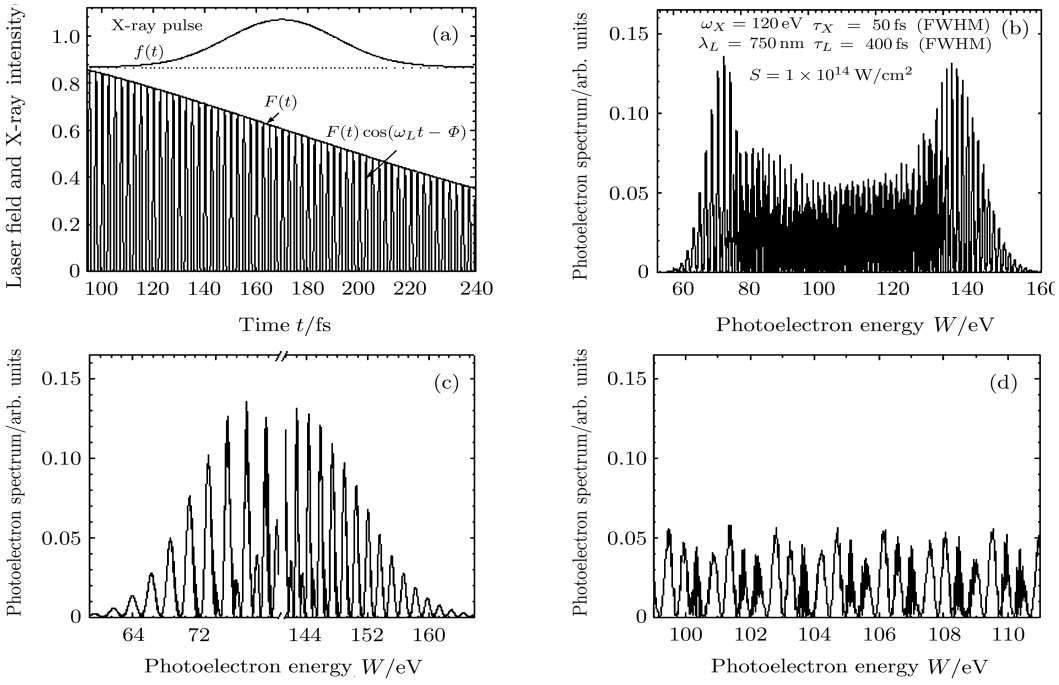


Fig.1. (a) Illustration of cross correlation between a 750 nm, 400 fs (FWHM) laser and a monochromatic 120 eV, 50 fs (FWHM) x-ray pulse. The laser related functions and x-ray intensity profile $f(t)$ are shown. (b) PES quantum-mechanically calculated with a laser peak intensity $S = 1 \times 10^{14}\,\mathrm{W/cm^2}$. (c) and (d) Expanded areas of the PES shown in (b).

1(b) shows the PES quantum-mechanically calculated with Eq.(2) at $\theta = 0°$. It is composed of many separated peaks. From Fig.1(b), we see the asymmetry of the whole PES particularly in low and high energy regions. Figures 1(c) and 1(d) exhibit the expanded areas of the PES. They clearly show local details of the PES. Unlike the asymmetry shown in Fig.1(c), the peak density of the PES is approximately uniform in the middle of the PES. Physically, the comb-like structures and asymmetry of the PES reflect the quantum interferences between the electron wave packets generated at different times.

The peak heights of Fig.1(b) are shown by open circles in Fig.2. Solid line in Fig.2 presents the classical predictions of the PES. Obviously, most peak heights are much higher than classical predictions, and the symmetry of the whole PES is better than the classical predicted one. Besides, the energy range of the PES is almost the same as the classical predicted one. Of course, from the quantum-mechanical point of view, there are photoelectrons located outside the classical predicted energy range. Calculations show that the height and the width of each peak as well as the number of peaks depend on the laser and the x-ray parameters.

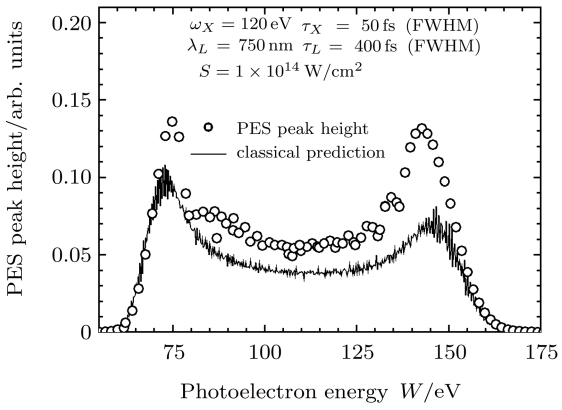


Fig.2. Peak heights of quantum-mechanically calculated PES (open circles) and classical predictions (thin solid line).

According to the semiclassical model for an atom in a strong laser field,[11] the final energy of a photoelectron moving at $\theta = 0°$ is $W(t) = W_0 + 2U_0F^2(t)\sin^2(\varpi_\mathrm{l}t + \Phi) + \sqrt{8U_0W_0}F(t)\sin(\varpi_\mathrm{l}t + \Phi)$, where t denotes the photoelectron birth time, U_0 is the ponderomotive energy of the laser field, and $W_0 = \varpi_\mathrm{x} - I_p$ is the initial kinetic energy of the photoelectron. Therefore, the minimum energy and the maximum energy of the PES are $W_\mathrm{min} = W_0 + 2U_0F^2(t_1) - \sqrt{8U_0W_0}F(t_1)$ and $W_\mathrm{max} = W_0 + 2U_0F^2(t_1) + \sqrt{8U_0W_0}F(t_1)$, respectively, where t_1 is the start time of the x-ray pulse. Thus, the classical predicted energy range is $2\sqrt{8U_0W_0}F(t_1)$. The energy ranges of the PESs calculated at different laser intensities and x-ray photon energies (e.g. Figs.1(b) and 3(a)) accord with the above estimations.

Figure 3(a) shows the PES calculated at $\lambda_\mathrm{l} = 750\,\mathrm{nm}$, $\tau_\mathrm{l} = 400\,\mathrm{fs}$, $\varpi_\mathrm{x} = 408\,\mathrm{eV}$ and $\tau_\mathrm{x} = 50\,\mathrm{fs}$. Figures 3(b) 3(c) and 3(d) show the expanded areas of the PES. Here, $\varpi_\mathrm{x} = 408\,\mathrm{eV}$ is in the middle of the x-ray energy at the water window (283.7–532.1 eV). From these figures, we see that the symmetry of the whole PES is better than that of Fig.1(b). Calculations indicate that the symmetry of PES is improved as the x-ray photon energy increases. Figure 3(b) shows the details in the middle of the PES. The peak density is much larger than that of Fig.1(d), and the uniformity is better. Figure 3(b) also shows peak groups, each with several small peaks. Different from the calculations at low x-ray photon energy in Fig.1(c), Figs.3(c) and 3(d) show some envelopes (lines denoted by S_1 and S_2 in Fig.3(c) and S_4 and S_5 in Fig.3(d)) of side-peaks beside the main peak (denoted by S_0 in Fig.3(c) and S_3 in Fig.3(d)). From Figs.3(c) and 3(d) it follows that the main peak heights (S_0 in Fig.3(c) and S_3 in Fig.3(d)) are much higher than the side peak heights at low and high energy regions of the PES, respectively.

In order to see how the main peak heights change as the x-ray photon energy varies in a small range, the expanded areas of PESs (denoted by A, B, C) are shown in Fig.4, which are calculated at $\lambda_\mathrm{l} = 750\,\mathrm{nm}$, $\tau_\mathrm{l} = 400\,\mathrm{fs}$, $\tau_\mathrm{x} = 50\,\mathrm{fs}$, and $\varpi_\mathrm{x} = (407, 408, 409)\,\mathrm{eV}$, respectively. Obviously, as the x-ray photon energy has a small shift, e.g. $\Delta\varpi_\mathrm{x} = \pm 1\,\mathrm{eV}$ for $\varpi_\mathrm{x} = 408\,\mathrm{eV}$ (see the inset of Fig.4, where a solid Gaussian shaped line illustrates an energy distribution of the photons), the position of each peak is just shifted by $\pm 1\,\mathrm{eV}$. This is an interesting feature that can be used to estimate the diffusions of the measured PES excited by a narrow bandwidth femtosecond x-ray pulse.

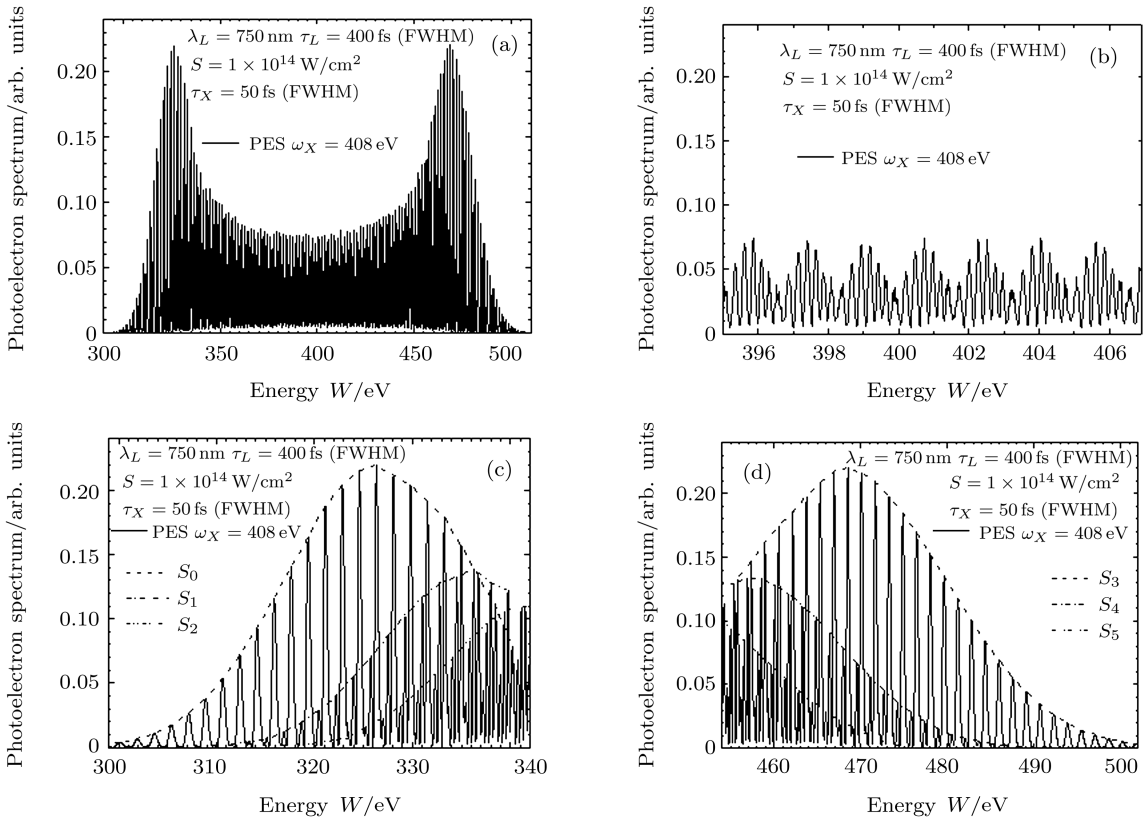


Fig.3. (a) Solid line: PES calculated at $\lambda_\text{l} = 750\,\text{nm}$, $\tau_\text{l} = 400\,\text{fs}$, $\varpi_\text{x} = 408\,\text{eV}$ and $\tau_\text{x} = 50\,\text{fs}$. (b), (c) and (d) Expanded areas of (a). Solid lines in (b), (c) and (d): PES. Dashed lines in (c) and (d): envelopes of main peaks. Dashed-dotted lines in (c) and (d): envelopes of side-peaks. Dashed-dotted-dotted lines in (c) and (d): envelopes of side-peaks.

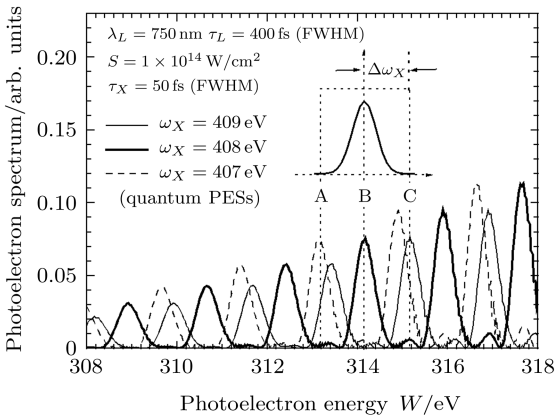


Fig.4. Expanded areas of PESs (denoted by A, B, C) calculated at $\lambda_\text{l} = 750\,\text{nm}$, $\tau_\text{l} = 400\,\text{fs}$, $\tau_\text{x} = 50\,\text{fs}$, and $\varpi_\text{x} = (407, 408, 409)\,\text{eV}$, respectively.

5. Conclusions

Calculations show that the PES excited by a femtosecond x-ray pulse is composed of a number of small peaks. The number, the width and the density of peaks depend on all the laser and x-ray parameters. As the x-ray photon energy increases, the symmetry of the PES and the uniformity of the peak density become better. Study also shows that the heights of main and side peaks depend on the laser and the x-ray pulse properties. As the duration of x-ray pulse decreases less than 0.4 fs, the comb-like structures of PES disappear. These interesting features can be used to reconstruct the x-ray pulse properties from the measured PES.

Acknowledgment

The author is grateful to Haiping He for assistance.

References

[1] Drescher M, Hentschel M, Kienberger R, Tempea G, Spielmann C, Reider G A, Corkum P B and Krausz F 2001 *Science* **291** 1923

[2] Hentschel M, Kienberger R, Spielmann C, Reider G A, Milosevic N, Brabec T, Corkum P B, Heinzmann U, Drescher M and Krausz F 2001 *Nature* **414** 509

[3] Drescher M, Hentschel M, Kienberger R, Uiberacker M, Yakovlev V, Scrinzi A, Westerwalbesloh T, Kleineberg U, Heinzmann U and Krausz F 2002 *Nature* **419** 803

[4] Kienberger R, Goulielmakies E, Uiberacker M, Baltuska A, Yakovlev V, Bammer F, Scrinzi A, Westerwalbesloh T, Kleineberg U, Heinzmann U, Drescher M and Krausz F 2004 *Nature* **427** 817

[5] Constant E, Taranukhin V D, Stolow A and Corkum P B 1997 *Phys. Rev.* A **56** 3870

[6] Dinu L C, Muller H G, Kazamias S, Mullot G, Augé F, Balcou P, Paul P M, Kovačev M, Breger P and Agostini P 2003 *Phys. Rev. Lett.* **91** 063901

[7] Mairesse Y and Quéré F 2005 *Phys. Rev.* A **71** 3124

[8] Itatani J, Quéré F, Yudin G L, Ivanov M Y, Krausz F and Corkum P B 2002 *Phys. Rev. Lett.* **88** 173903

[9] Kitzler M, Milosevic N, Scrinzi A, Krausz F and Brabec T 2002 *Phys. Rev. Lett.* **88** 173904

[10] Quéré F, Itatani J, Yudin G L and Corkum P B 2003 *Phys. Rev. Lett.* **90** 073902

[11] Ge Y C 2008 *Chin. Phys.* B **17** 2072

[12] Lewenstein M, Balcou P, Ivanov M Y, L'Huillier A and Corkum P B 1994 *Phys. Rev.* A **49** 2117

[13] Brabec T and Krausz F 2000 *Rev. Mod. Phys.* **72** 545